Journal of Hydrology 486 (2013) 57–70

Contents lists available at SciVerse ScienceDirect

Journal of Hydrology

journal homepage: www.elsevier.com/locate/jhydrol

Significant coherence for groundwater and Rayleigh waves: Evidence in spectral response of groundwater level in Taiwan using 2011 Tohoku earthquake, Japan

David Ching-Fang Shih [a,*], Yih-Min Wu [b], Chien-Hsin Chang [c]

[a] Institute of Nuclear Energy Research, P.O. Box 3-7, Longtan 32546, Taiwan
[b] Department of Geosciences, National Taiwan University, Taipei 10617, Taiwan
[c] Central Weather Bureau, Taipei 10048, Taiwan

ARTICLE INFO

Article history:
Received 14 January 2013
Accepted 18 January 2013
Available online 29 January 2013
This manuscript was handled by Corrado Corradini, Editor-in-Chief, with the assistance of Fritz Stauffer, Associate Editor

Keywords:
Groundwater
Seismic
Earthquake
Rayleigh waves
Spectral analysis

SUMMARY

It was found that groundwater can be fluctuated by a variety of disturbances. For instance, seismic activity inducing the dilatation of earth can disturb groundwater level fluctuation as observed in groundwater wells. In this research, spectral analysis in the frequency domain was used to quantitatively evaluate coherence between groundwater head fluctuations and the ground motions recorded in Taiwan from a distant earthquake, the 2011 Tohoku earthquake in northern Honshu, Japan with magnitude of 9. The relationship between groundwater fluctuations and the decomposed ground motions of Rayleigh waves are clearly identified. By analyzing autospectral density, cross-spectral density, and resultant coherence for the seismograms and groundwater head, it was found that the Rayleigh waves dominated the groundwater fluctuations at period of about 21–32 s for six pair of groundwater and seismograms of broadband distributed around Taiwan; fluctuations of groundwater are highly coherent with the radial and vertical components of ground motions. Our analysis also shows the time from event to station for Rayleigh waves ranged from 780 to 900 s approximately. Wave parameter for seismic event to station of groundwater and seismograms were also identified as 3.0–3.5 km/s and 64–110 km for wave velocity and wave length, respectively. The relationship of groundwater fluctuations and ground motions induced by seismic activity become feasible to assess using spectral analysis.

1. Introduction

The study demonstrates that the polarities of the observed coseismic water-level and river discharge changes are in good agreement with those of the static volumetric strain calculated by a dislocation model, using the well-constrained rupture model of the seismogenic Chelungpu fault (Lee et al., 2002). Analysis of strong-motion instrument recordings in Seattle, Washington, resulting from the 2002 M_w 7.9 Denali, Alaska, earthquake reveals that amplification in the 0.2–1.0 Hz frequency band is largely governed by the shallow sediments both inside and outside the sedimentary basins beneath the Puget Lowland (Barberopoulou et al., 2006). For the great Sumatra earthquake of M_w 9.3 on 2004, Chadha et al. (2008) indicated that large water level changes are attributed to the dynamic strain induced by the passage of seismic waves, most probably long-period surface waves. The Sumatra–Andaman Islands Earthquake with magnitude 9 on 26 December 2004 at 00:58:53.45 UTC was used as the seismic disturbance to estimate groundwater storage in well-aquifer system located in the eastern Taiwan (Shih, 2009).

The studies have observed that water level fluctuations in an aquifer-well system demonstrated strong correlations to nearby boundary disturbances (Shih et al., 2008a; Rotzoll et al., 2008). Cooper et al. (1965) studied the water level response to pressure-head fluctuations due to dilatation of the aquifer and to vertical motion of the well-aquifer system induced by seismic waves. The response of a confined well-aquifer system to tidal dilatations, consisting of the earth tidal dilatation, the harmonic tidal dilatation, and the ocean tidal dilatation, has also been demonstrated (Robinson and Bell, 1971). Shih (2009) derived the spectral relationship between groundwater level and the vertical components of seismic Rayleigh waves. By using the derived spectral relationship, the groundwater storage properties, storage coefficient and specific storage were evaluated. In the study by Shih (2009), the Sumatra–Andaman Islands Earthquake with magnitude 9 on 26 December 2004 was used as the seismic activation to the well-aquifer system located in the eastern Taiwan while a nearby groundwater monitoring well and a broadband seismic station were served as the receivers. The resultant spectral estimates were used to deter-

* Corresponding author. Tel.: +886 2 82317717x5750; fax: +886 3 4711411.
E-mail address: cfshih@iner.gov.tw (D.Ching-Fang Shih).

0022-1694/$ - see front matter © 2013 Elsevier B.V. All rights reserved.
http://dx.doi.org/10.1016/j.jhydrol.2013.01.013

mine the storage coefficient and specific storage of the case site to be on the order of 10^{-3} and 10^{-4} (m^{-1}), respectively.

It is known that short-term hydraulic head in an aquifer is strongly affected by incident earthquake seismic waves since the pioneering study by Cooper et al. (1965). In this study, six pairs of groundwater level and seismogram in the Taiwan have been collected utilizing the seismic source located in the eastern Honshu, Japan. Generally, the fluctuations of groundwater level in the study aquifer can be traced by the three-component in seismograms. However, the relationships behind those phenomena are still not fully identified in the present time. Therefore, this research aims to provide demonstrative evidence by analyzing the correlation between groundwater level and the seismic Rayleigh waves in vertical and radial components. We interpreted the structure and examined the particle motions of Rayleigh waves. Spectral analysis was also used to identify the dominant period for groundwater fluctuations and the segments associated with Rayleigh wave observations. Coherence between groundwater fluctuation and components of seismograms is well discussed and indicative evidence is then demonstrated.

2. Background information

The USGS has updated the magnitude of the March 11, 2011 (05:46:23 UTC), Tohoku earthquake in northern Honshu, Japan, to 9.0 from the previous estimate of 8.9. Independently, Japanese seismologists have also updated their estimate of the earthquake's magnitude to 9.0. This magnitude places the earthquake as the fourth largest in the world since 1900 and the largest in Japan since modern instrumental recordings began 130 years ago. The earthquake event with magnitude 9.0 near the east coast of Honshu, Japan, is adopted as the seismic source to the groundwater and broadband stations of Taiwan (Table 1).

Taiwan is a member of the Ryukyu–Taiwan–Philippine arc chain rimming the western border of the Pacific Ocean. The tectonic evolution of Taiwan can be attributed either to the development of classic geosynclinal cycles or to the interaction of crustal plates. In the geosynclinal model, Taiwan is formed by a typical mobile or orogenic Cenozoic geosynclinal deposition on a pre-Tertiary metamorphic basement filled with Tertiary sediments to a thickness of more than 10,000 m (Ho, 1982). In the plate tectonic model, the main island of Taiwan is situated on the junction between the continental Eurasian plate on the west and the oceanic Philippine Sea Plate on the east. Taiwan can thus be divided into two major geologic or tectonic provinces, separated by a linear and narrow fault-bounded valley that marks the collision suture of the two converging plates (Ho, 1982).

As the schematic model showing continent-arc collision and plate tectonic setting of Taiwan (Shih et al., 2008b), the Central Ridge pass through the Taiwan island, studied groundwater of aquifer are denoted as groups (I), (II), (III), and (IV) (Fig. 1). Six sets of groundwater level and seismogram were collected from Central Weather Bureau (CWB) of Taiwan (Table 1). For the groundwater stations, TUN and HWA are located in the eastern of Taiwan while DON, LIU, NAB, and CHI in the western; they are arranged from north to south, respectively. Geologic logging shows that groundwater well all are tapped in confined aquifer (Table 1). Correspondent seismogram stations are NANB, HWAH, WGK, TPUB, SGS, and MASB, respectively. In which NANB, TPUB, and MASB are stations of the Broadband Array in Taiwan for Seismology (BATS). In group (I), HWA and HWAH are located on the northern of Longitudinal Valley in Coast Range, it is near the eastern of Taiwan. For the same group, TUN is located on ILan Plain. ILan Plain is a triangular plain on the northern coast, opening to the Pacific Ocean toward the northeast. The two other sides are fringed by high mountains composed mainly of Miocene to Paleogene slate. In tectonic analysis, the ILan Plain marks the western termination of Okinawa trough that extends from Japan towards the northern end of Taiwan. In group (II), DON and WGK are located near the boundary between the Western Coastal Plain and the Central Range of Taiwan. From the well data, in the Western Coastal Plain area, it is apparent that

Table 1
Information of seismogram and groundwater station.

Type	Station	N (°)	E (°)	Altitude (m)	Distance to event (km)	Control seismogram station
Honshu event		38.32200	142.36900	−32000.00		
Groundwater	TUN	24.74371	121.78962	3.79	2467.08743	NANB
	HWA	23.97538	121.61333	16.09	2539.17236	HWAH
	DON	23.68489	120.56993	75.41	2639.63627	WGK
	LIU	23.22545	120.35059	26.87	2691.50476	TPUB
	NAB	23.06913	120.34870	42.77	2703.77012	SGS
	CHI	22.59242	120.61441	26.78	2721.43177	MASB
						Geology
Seismogram	NANB	24.42750	121.74980	112.00	2494.17185	Rock
	HWAH	23.97700	121.60560	−294.00	2539.62157	Alluvial
	WGK	23.68440	120.57030	75.00	2639.64595	Sedimentary
	TPUB	23.30050	120.62960	370.00	2664.80742	Siltstone
	SGS	23.08040	120.59080	278.00	2684.83066	Sedimentary
	MASB	22.61190	120.63280	139.00	2718.53463	–
		Level of top casing (m)	Screen interval (m) Well length (m)	Aquifer thickness (m)	Hydraulic conductivity (cm/s)	Aquifer/soil type
Groundwater well	TUN	3.79	130–150 180	19	–	Confined/sand
	HWA	16.09	161–185 191	24	6.8×10^{-6}	Confined/gravel
	DON	75.41	222–252 270	30	–	Confined/gravel
	LIU	26.87	204–222 250	42	–	Confined/sand
	NAB	42.77	135–147 250	9	–	Confined/sand
	CHI	26.78	158–170, 183–191 251	17, 8	–	Two layers, confined/gravel

–: Lack of data; diameter of well all are 0.1524 m.

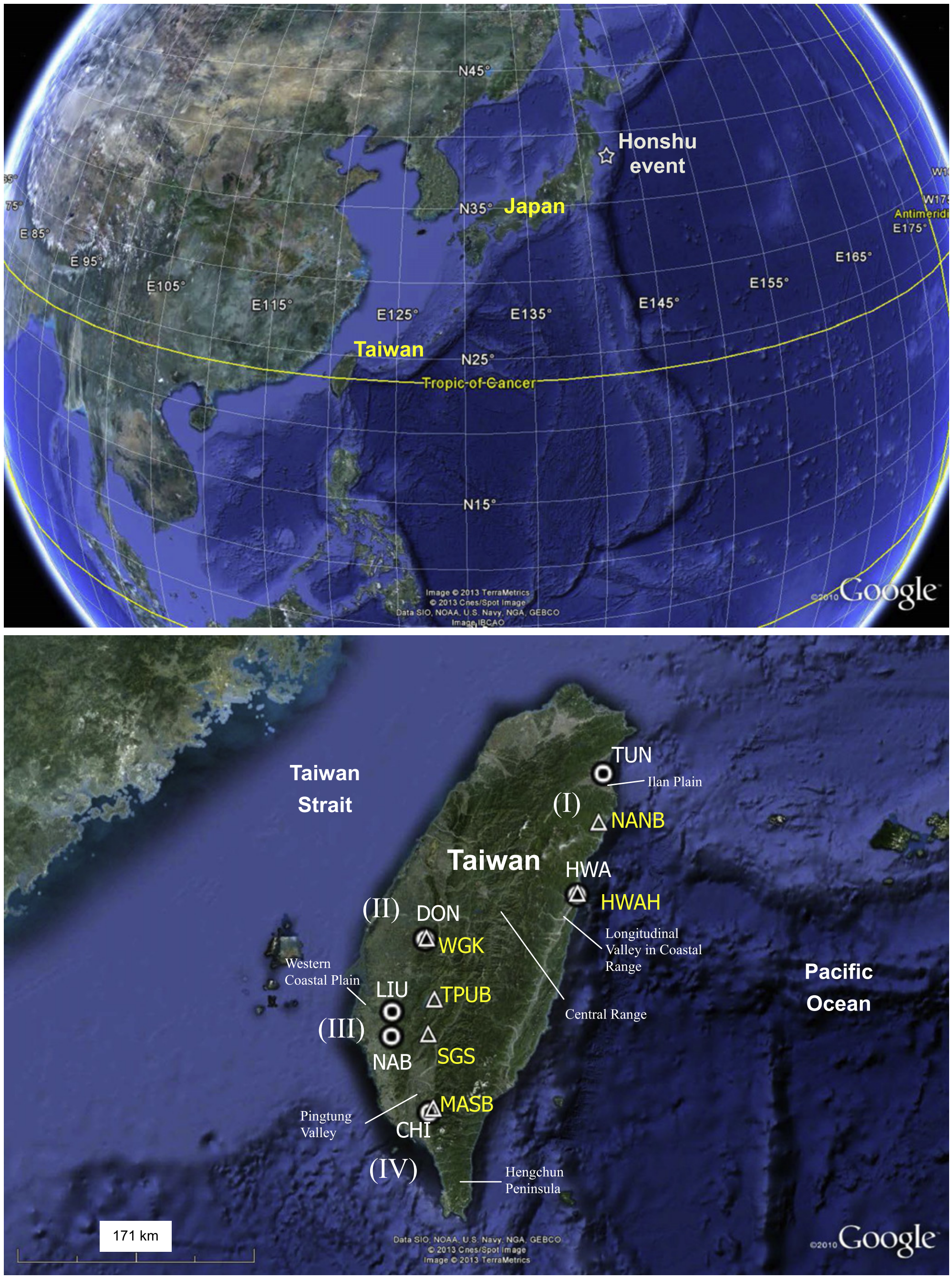

Fig. 1. Map shows the epicenter location of the 2011 Tohoku earthquake in northern Honshu (Japan), groundwater monitoring station and seismic station; Map sources: Google Earth (2013).

the Neogene rocks in the western basin overstep basement rocks of different geologic ages. In general, they can be divided into categories as Paleozoic, Cretaceous, and Paleocene or Eocene/Paleocene. In group (III), LIU/TPUB and NAB/SGS pairs are quite similar, groundwater station LIU and NAB are located on the Coastal Plain of Taiwan while seismological monitoring station TPUB and SGS sited on the west-south part of Central Range. In group (IV), CHI and MASB are located on the Pingtung Valley and its northern boundary to the Central Ridge of Taiwan, respectively. The Pingtung Valley in southern Taiwan is located between the noble Central Range on the east and low hilly upland on the west. The Central Range extends immediately southward, forming the Hengchun Peninsula east of the Pingtung Valley. The Pingtung Valley is a sediment-filled trough, having a north-south of 55 km and a east-west width averaging 20 km. As the above stated, it implies that the targeted aquifer of our research are site specific for different geologic setting.

Radial (x), transverse (y) and vertical (z) components of Rayleigh waves observed in seismograms from Honshu event to the groundwater and broadband station are decomposed from original east, north, and vertical (E, N, Z) components in seismogram; in which, z and Z are identical. Vertical component (Z) in seismogram stations are controlled set for the groundwater level. In order to analyze the response of groundwater in the well-aquifer system to seismic waves, Tohoku earthquake with magnitude of 9.0 in northern Honshu, Japan, occurred on March 11, 2011 at 05:46:23 UTC is chosen as the seismic source. Fig. 2 was shown for water level of groundwater station DON and x–

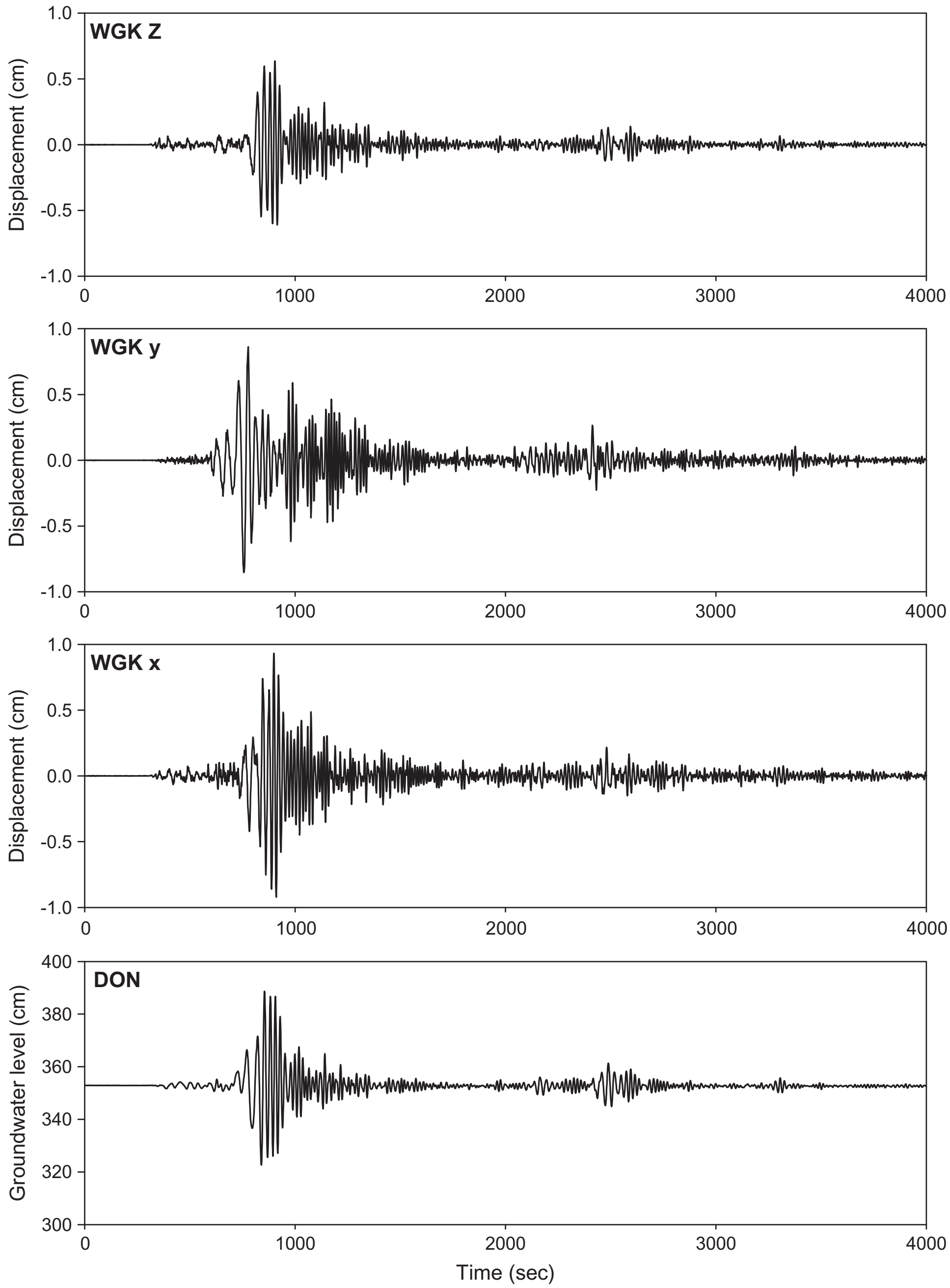

Fig. 2. Time series for groundwater station DON and three components of seismogram for seismic station WGK.

y–Z components of controlled seismogram station WGK. They demonstrate significant fluctuation versus time from 800 to 1500 s after Honshu event, especially groundwater level of DON and x and Z components of WGK present similar type of variations.

Generally, seismograms are dominated by those of large and long period waves that arrive after the P and S waves. These waves are surface waves whose energy is most concentrated near the earth's surface. As a theoretical result of geometric spreading, their energy propagates two-dimensionally and decays with a function of r^{-1}, where r is the distance from the source. The energy of P and S waves, so called body waves, spreads three-dimensionally and decays approximately with a function of r^{-2}. Thus, surface waves prevail on seismograms at greater distances from the source (Stein and Wysession, 2003).

Seismograms in the east-west and north-south directions recorded by a three-component seismometer are commonly rotated to the directions of radial and transverse directions for seismic phase identifications. In this study, we used x, y, and Z representing the directions of radial, transverse, and vertical, respectively.

One type of surface waves is Rayleigh wave, which is a combination of P and SV motions and propagates in the x–Z plane with its displacement on the plane. Because the vertical and radial components of Rayleigh wave motion are out of phase in the x–Z plane, the particle motions at a point on the free surface as a function of time are found to be retrograde ellipse (Stein and Wysession, 2003). The particle moves in the opposite direction of wave propagation at the top of the ellipse. It concludes that the radial component can dispread the group of Rayleigh waves on surface horizontally, and the vertical component fluctuates groundwater head in the z direction. Cooper et al. (1965) found that Rayleigh waves cause larger fluctuation in wells than other wave that has been identified. Since it produces both dilatation and vertical motion, a comparison of the variation of pressure head of groundwater with the vibration of land surface due to a Rayleigh wave can be studied. Another type of surface waves is Love wave, which is produced by *SH*-wave reverberations. Because the displacement of Love wave is parallel to the y axis, Love wave motion is not concerned in this study.

Time series of Rayleigh wave for seismogram stations was demonstrated in Fig. 3, phase lag between x and Z component are apparent for all stations. The radial and vertical (x and Z) trajectory are also shown (Fig. 4). Because the radial and vertical components are out of phase for Rayleigh wave propagation, elliptical retrograde motions indicate the characteristics of Rayleigh wave propagation (Stein and Wysession, 2003). A particle will move in the opposite direction of wave propagation at the top of the ellipse. Therefore, the time window of Rayleigh wave observation is determined. Fig. 5 represent the

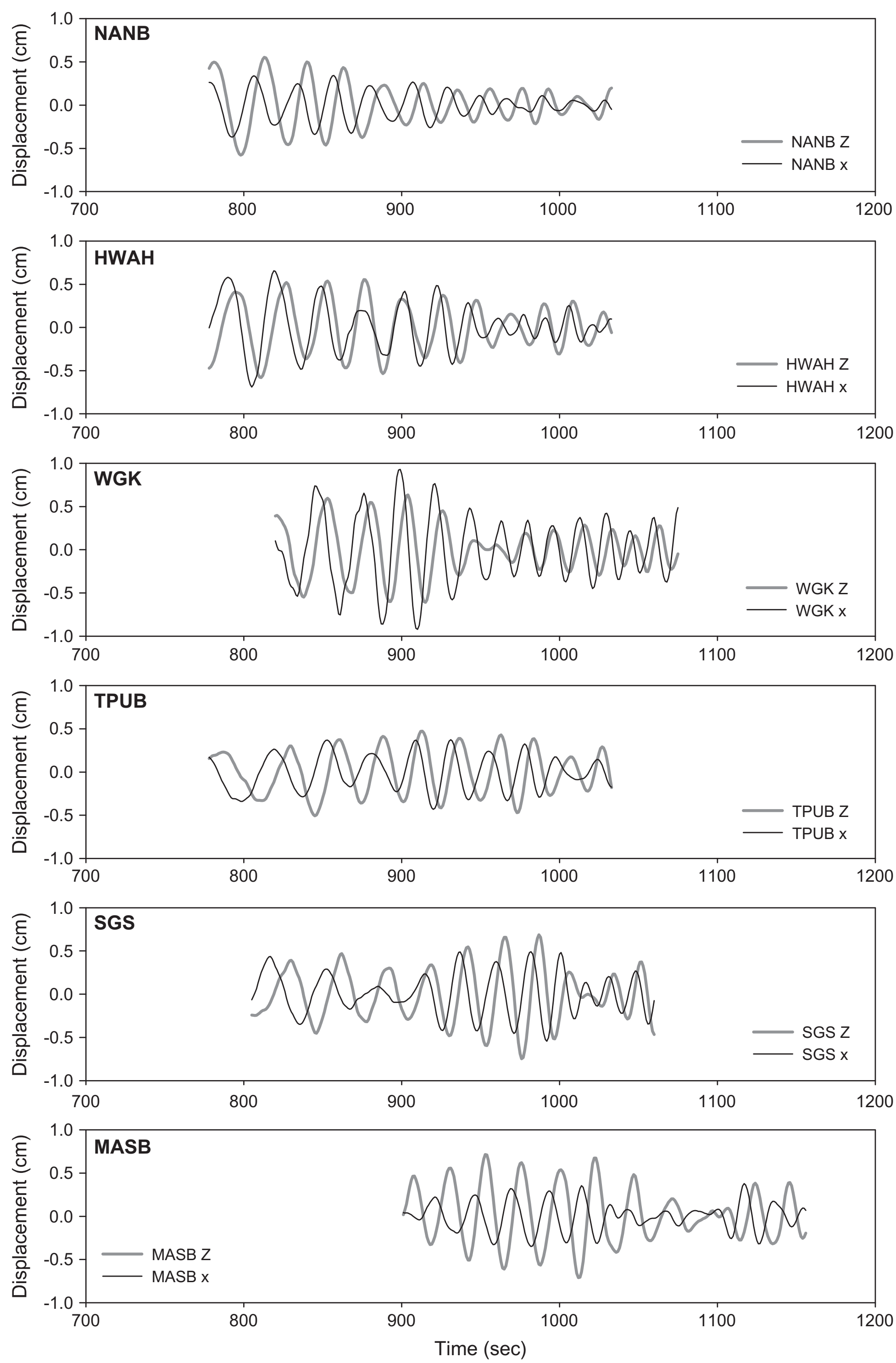

Fig. 3. Seismograms observed at six seismic station; presented in the radial and vertical component x and Z, respectively.

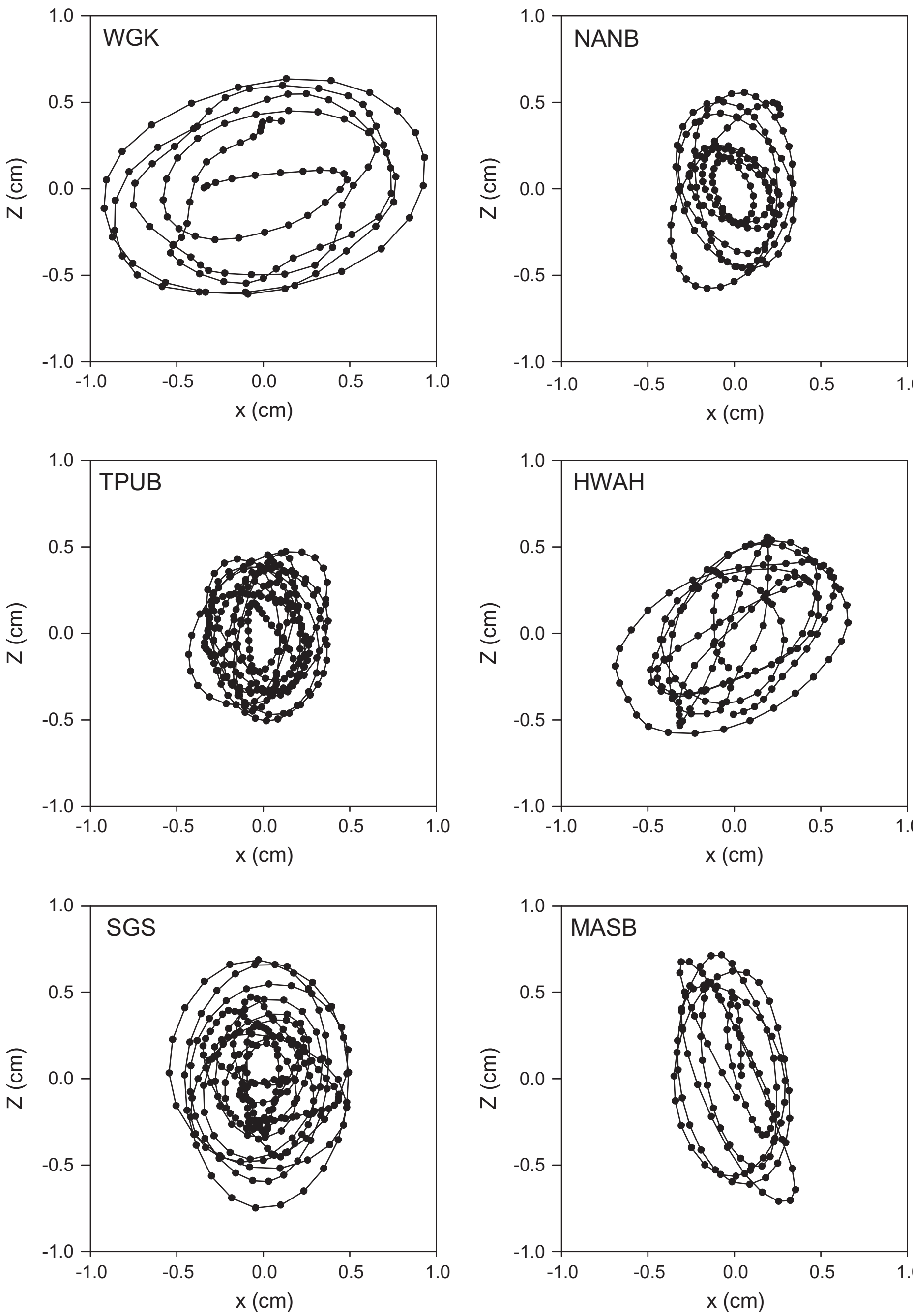

Fig. 4. Radial (x) and vertical (Z) trajectory of the decomposed seismograms for Rayleigh wave propagation.

radial component of seismogram station and groundwater station. Due to different layout for groundwater and its control seismogram, phase lags are also comparable. Time series data are sampled for total 256 samples to identify the coherence for groundwater fluctuations and Rayleigh wave disturbance in the aquifer-well system using spectral analysis.

3. Spectral analysis

Spectral analysis in the time–frequency domain is a useful tool to evaluate characteristics of the embedded periodic fluctuations in time series. Applications of spectral analysis to identify frequency of groundwater fluctuation and phase propagation in tidal water level of aquifer and nearby coast water body have been demonstrated (e.g. Shih, 1999; Shih and Lin, 2004; Shih et al., 2008a). In this study, autospectral density is used to detect the strong signal in time series, while cross-spectral density and coherence are measurements to identify the intensity of specific target signals between two time series. The 95% confidence interval of autospectral density and non-zero coherence level for cross-spectral density are also evaluated in this study to identify significant components in frequency domain. Detailed presentation of the spectral techniques used in this study can be found in Bendat and Piersol (2000).

Considering a random variable in the time domain $x = x(t)$, the complex Fourier components can be expressed as

$$X(f) = \int_{-\infty}^{\infty} x(t)e^{-2\pi fti}dt \qquad (1)$$

where x is a random variable in the time domain, t is the elapsed time, f is the frequency, X is the complex Fourier components in

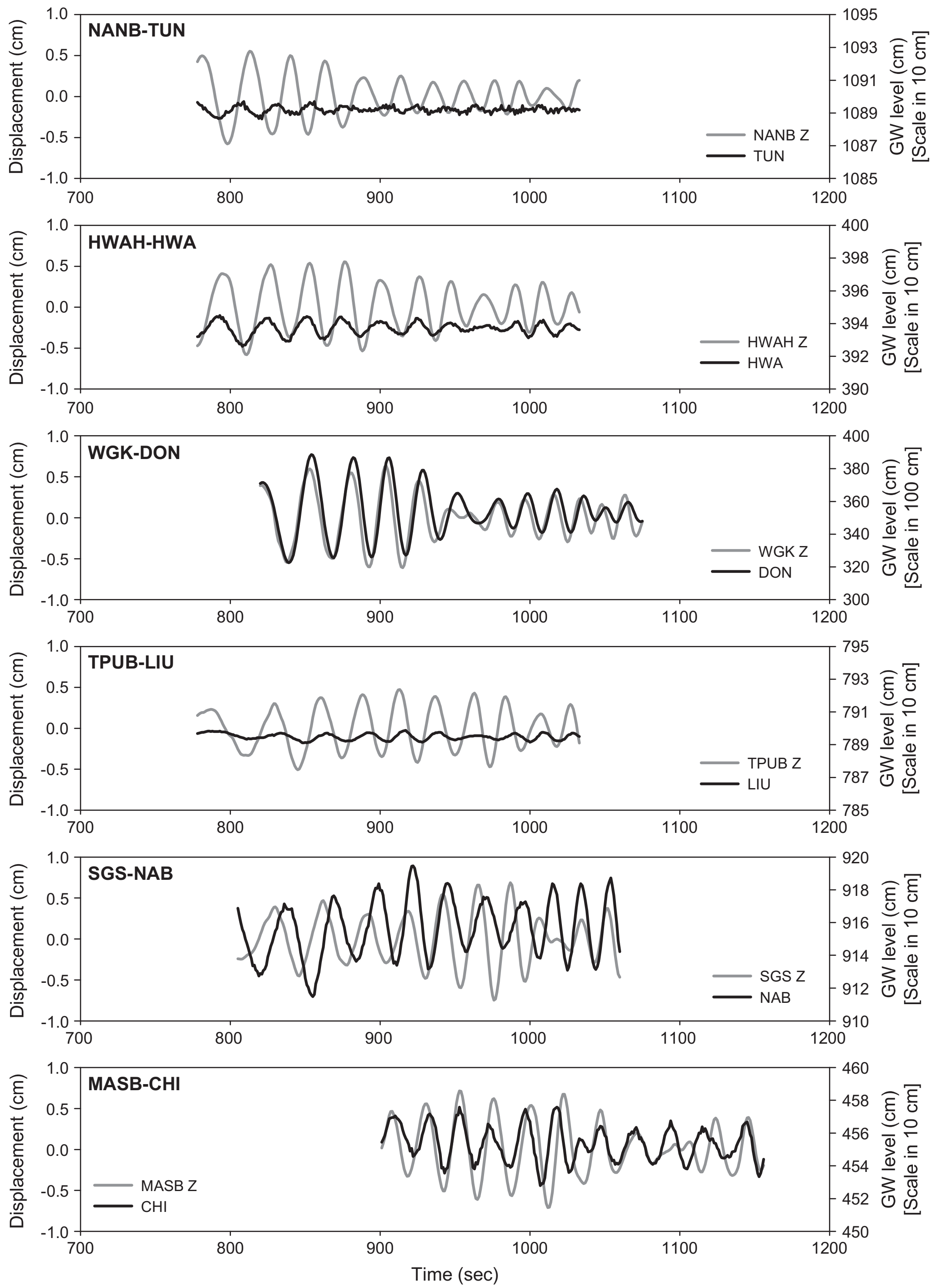

Fig. 5. Time series of groundwater level and vertical (Z) component of seismograms.

the frequency domain, and i is $\sqrt{-1}$. In a practical application, let the finite time factor be incorporated in Eq. (1), which can be rewritten as

$$X(f,T) = \int_0^T x(t)e^{-2\pi fti}dt \quad (2)$$

where T is a finite time sequence.

It is obvious that the transformed component X is not only a function of frequency but also of the finite time length. For a small time period, Eq. (2) cannot be satisfied due to lack of statistical significance. If the time windows of seismic and groundwater head signals are too short for instance, the affected physical properties associated with seismic motions and water level fluctuations are discarded.

Consider a stationary time series $x(t)$ of a total length of T, and let $x(t)$ be divided into nd contiguous segments with each segment length of Ts, the two-sided autospectral density for each segment can be estimated by

$$S_{xx} = \frac{1}{T_s}|X(f, T_s)|^2 \tag{3}$$

By averaging each of the resulting components, a final smooth two-sided autospectral density can be obtained and it should satisfy the required statistical significance level (Bendat and Piersol, 2000).

Given Δt as the sampling rate in the time domain, the discrete frequency is defined as

$$f_k = \frac{k}{T_s} = \frac{k}{N\Delta t} \quad k = 0, 1, 2, \ldots, N-1 \tag{4}$$

where N is the length of segments. The smoothed, one-sided autospectral density is expressed as

$$\widetilde{G}_{xx} = \frac{2}{n_d N\Delta t}\sum_{i=1}^{n_d}|X_i(f_k)|^2 \quad k = 0, 1, 2, \ldots, \frac{N}{2} \tag{5}$$

In order to obtain the cross-spectral density in the frequency domain for two different time series, for example $x(t)$ and $y(t)$, the raw estimate of cross-spectral density for each sub-record is computed through Fourier components $X(f_k)$ and $Y(f_k)$ using

$$\widetilde{G}_{xy} = \frac{2}{n_d N\Delta t}\sum_{i=1}^{n_d}[X_i^*(f_k)Y_i(f_k)] \tag{6}$$

where $X^*(f_k)$ is the complex conjugate of $X(f_k)$, and $k = 0, 1, 2, \ldots, \frac{N}{2}$.

As previously mentioned, the smooth estimate of cross-spectral density and associated quantity for nd blocks of time segments can be expressed as

$$\widetilde{G}_{xy}(f_k) = \widetilde{C}_{xy}(f_k) - i\widetilde{Q}_{xy}(f_k) = |\widetilde{G}_{xy}(f_k)|e^{-i\tilde{\theta}_{xy}(f_k)} \tag{7}$$

$$\tilde{\theta}_{xy}(f_k) = \tan^{-1}[\widetilde{Q}_{xy}(f_k)/\widetilde{C}_{xy}(f_k)] \tag{8}$$

$$\tilde{\gamma}^2_{xy}(f_k) = \frac{|\widetilde{G}_{xy}(f_k)|^2}{\widetilde{G}_{xx}(f_k)\widetilde{G}_{yy}(f_k)} \tag{9}$$

where $\widetilde{C}_{xy}(f_k), \widetilde{Q}_{xy}(f_k), \tilde{\theta}_{xy}(f_k), \tilde{\gamma}^2_{xy}(f_k)$ are co-spectral density, quadrature-spectral density, phase angle, and squared coherence, respectively, for $k = 0, 1, 2, \ldots, \frac{N}{2}$.

The autospectral density using 95% confidence interval is then given as

$$\frac{n\widetilde{G}_{xx}(f_k)}{\chi^2_{n;0.05/2}} \leqslant \widetilde{G}_{xx}(f_k) \leqslant \frac{n\widetilde{G}_{xx}(f_k)}{\chi^2_{n;1-0.05/2}} \tag{10}$$

where $\chi^2_{n;\alpha}$ is the Chi-square distribution such that Probability $\left[\chi^2_n > \chi^2_{n;\alpha}\right] = \alpha$ for a percentage α with n degrees of freedom, where $n = 2n_d$ in this study (Bendat and Piersol, 2000). Then, the coherence with 95% confidence interval given by Bendat and Piersol (2000) is

$$1 - \frac{2\sqrt{2}(1-\tilde{\gamma}(f_k)^2)}{|\tilde{\gamma}(f_k)|\sqrt{n_d}} \leqslant \tilde{\gamma} \leqslant 1 + \frac{2\sqrt{2}(1-\tilde{\gamma}(f_k)^2)}{|\tilde{\gamma}(f_k)|\sqrt{n_d}} \tag{11}$$

Therefore, the 95% non-zero coherence significance level (NZC; Shih et al., 1999) can be derived as

$$\tilde{\gamma}(f_k) = |\tilde{\gamma}(f_k)| = \frac{\sqrt{n_d+32} - \sqrt{n_d}}{4\sqrt{2}} \tag{12}$$

4. Result and discussion

The records of three-component ground motions of Rayleigh waves and groundwater level from a distant earthquake was collected in this study. The isolated time window of Rayleigh wave portion has be selected by the analysis of particle motions on the x–Z plane. Before conducting the stationary spectral analysis presented in the previous section, descriptive statistics was used to evaluate the basic characteristics of the seismograms. Hence, normality assessment is performed using K–S test which Kurtosis and Kolmogorov–Smirnov distance (K–S distance) are derived (Peacock, 1983; Lopes et al., 2007) to fit the normal Gaussian distribution. K–S distance is the maximum cumulative distance between the cumulative distributions of data and of a Gaussian distribution, while kurtosis is a measure of the observed peaked or flat distribution deviating from a normal distribution. A normal distribution has kurtosis equal to zero. The Shapiro–Wilk W-statistic tests the null hypothesis that data was sampled from a normal distribution (Shapiro and Wilk, 1965). Small values of W indicate a departure from normality. Table 2 shows that groundwater and component of broadband represent deviation of zero for Kurtosis and small value of W. They indicate that the data varies significantly from the expected pattern assuming the data was drawn from a population with a normal distribution; that is, invoke failed normality test. It implies that the process of time series data for stationary spectral analysis is needed.

Table 2
Descriptive statistics for groundwater level and broadband x–Z components.

	Skewness	Kurtosis	K–S distance	K–S probability	Shapiro–Wilk W-statistic	Shapiro–Wilk probability
NANB Z	0.0123	−0.290	0.0379	0.473	0.989	0.040
NANB x	−0.0668	−0.434	0.0440	0.261	0.988	0.026
TUN[a]	−0.2280	0.181	0.0507	0.109	0.990	0.082
HWAH Z	−0.0361	−0.950	0.0610	0.022	0.977	<0.001
HWAH x	0.0124	−0.282	0.0443	0.252	0.991	0.105
HWA[a]	−0.2960	−0.297	0.0424	0.310	0.987	0.021
WGK Z	−0.0009	−0.442	0.0268	0.848	0.989	0.058
WGK x	0.0207	−0.458	0.0469	0.184	0.992	0.180
DON[a]	0.1660	−0.225	0.0380	0.468	0.983	0.004
TPUB Z	−0.0566	−1.163	0.0775	<0.001	0.961	<0.001
TPUB x	−0.0042	−1.021	0.0666	0.008	0.972	<0.001
LIU[a]	−0.0450	−1.006	0.0753	0.001	0.972	<0.001
SGS Z	0.0021	−0.597	0.0604	0.025	0.990	0.088
SGS x	−0.0078	−0.641	0.0299	0.768	0.988	0.030
NAB[a]	−0.0561	−0.800	0.0769	<0.001	0.983	0.004
MASB Z	0.0888	−0.718	0.0570	0.043	0.985	0.008
MASB x	−0.0728	−0.396	0.0489	0.142	0.984	0.006
CHI[a]	0.0313	−0.738	0.0505	0.113	0.986	0.015

[a] Groundwater.

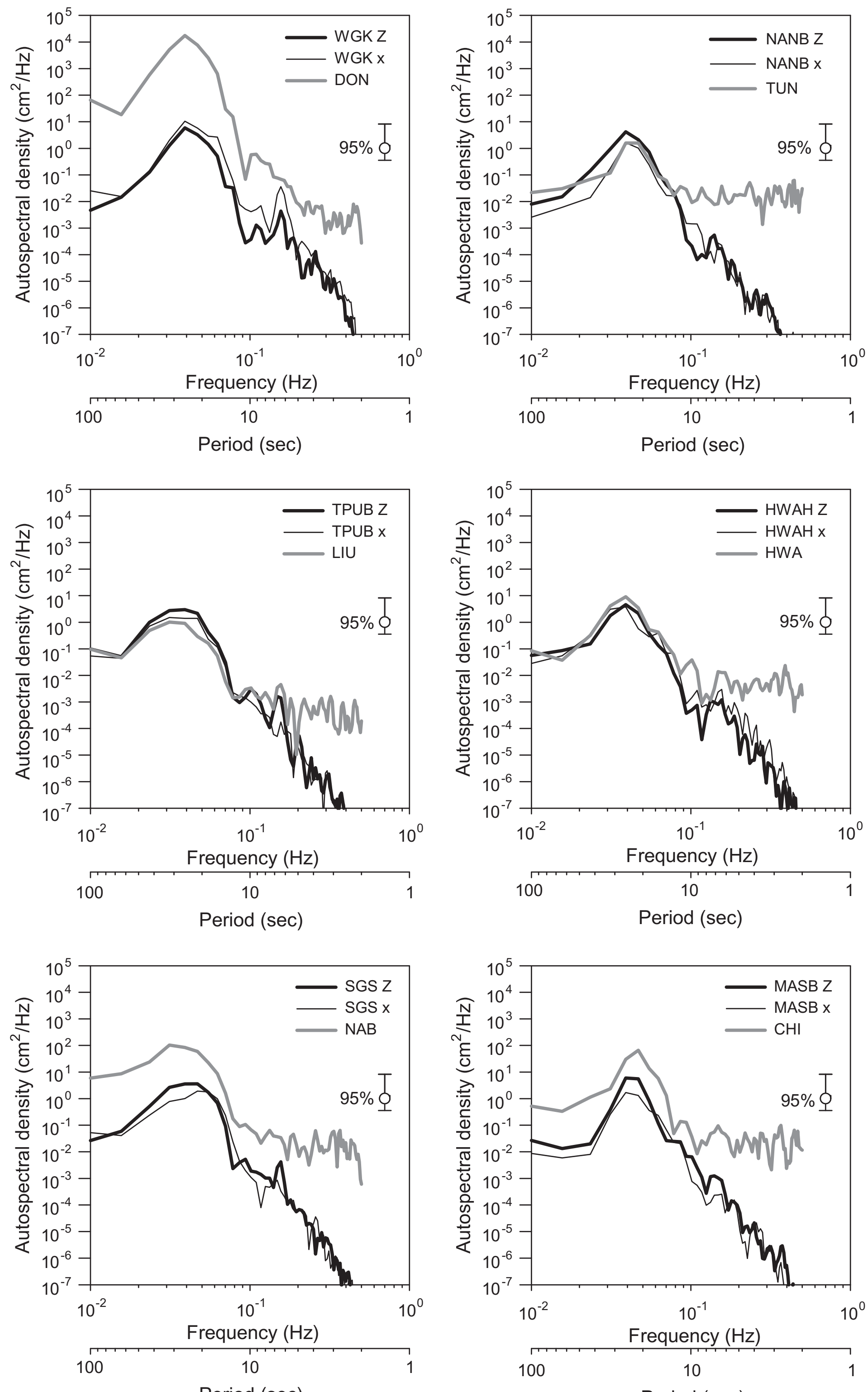

Fig. 6. Autospectral density in the frequency domain.

In order to reduce random error of spectral density function, the data are divided into 2 sub-records with each 128 samples to obtain a smooth estimate. To suppress the unnecessary variations for Rayleigh waves in the time series, removal of linear trend is adopted on each sub-record using the least-square method, while the Hanning window is used to suppress leakage problem for spectral density (Bloomfield, 1976). The resolution of discrete frequency is at 0.78125×10^{-2} Hz. The autospectral density with 95% confidence interval has the lower and the upper extremes of 0.3586 and 8.2573 cm^2/Hz, respectively. Non-zero coherence significant level is indicated to be 0.781. Although the confidence interval of the cross-spectral density is dependent on coherence at each discrete frequency interval, it is reasonable to evaluate the significant peak in cross-spectral density using

Table 3
Spectral analysis.

Seismogram (SM) / Groundwater (GW)	Distance to epicenter (km)	Frequency (Hz)	Period (s)	Auto-spectra (cm²/Hz) Z of SM	Auto-spectra (cm²/Hz) GW	Cross-spectra (cm²/Hz)	Coherence	Phase (°)	Time lag (s)
NANB **TUN**[a]	2494.17185 2467.08743	0.03906	25.60	4.18	1.59	2.54	0.99	−130.65	−9.29
HWAH **HWA**[a]	2539.62157 2539.17236	0.03906	25.60	4.61	9.15	6.44	0.99	−29.97	−2.13
WGK **DON**[a]	2639.64595 2639.63627	0.03906	25.60	5.93	17628.30	323.07	1.00	25.50	1.81
TPUB **LIU**[a]	2664.80742 2691.50476	0.03125	32.00	2.76	1.02	1.67	1.00	44.86	3.99
SGS **NAB**[a]	2684.83066 2703.77012	0.03125	32.00	2.65	103.39	16.39	0.99	91.87	8.17
MASB **CHI**[a]	2718.53463 2721.43177	0.04688	21.33	5.54	65.62	16.17	0.85	−14.62	−0.87

[a] Groundwater.

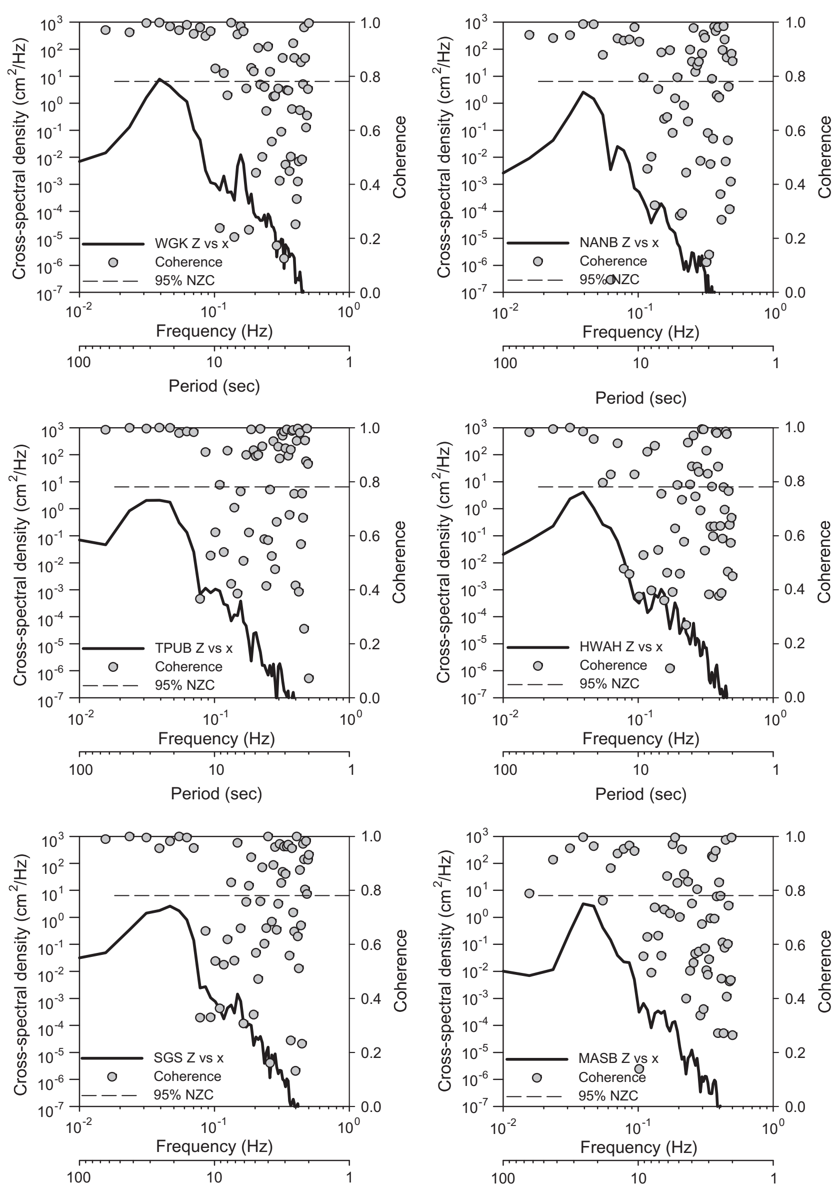

Fig. 7. Cross-spectral density in the frequency domain for *x* versus *Z* components of seismograms. The short dash lines indicate the 95% non-zero coherence level (NZC).

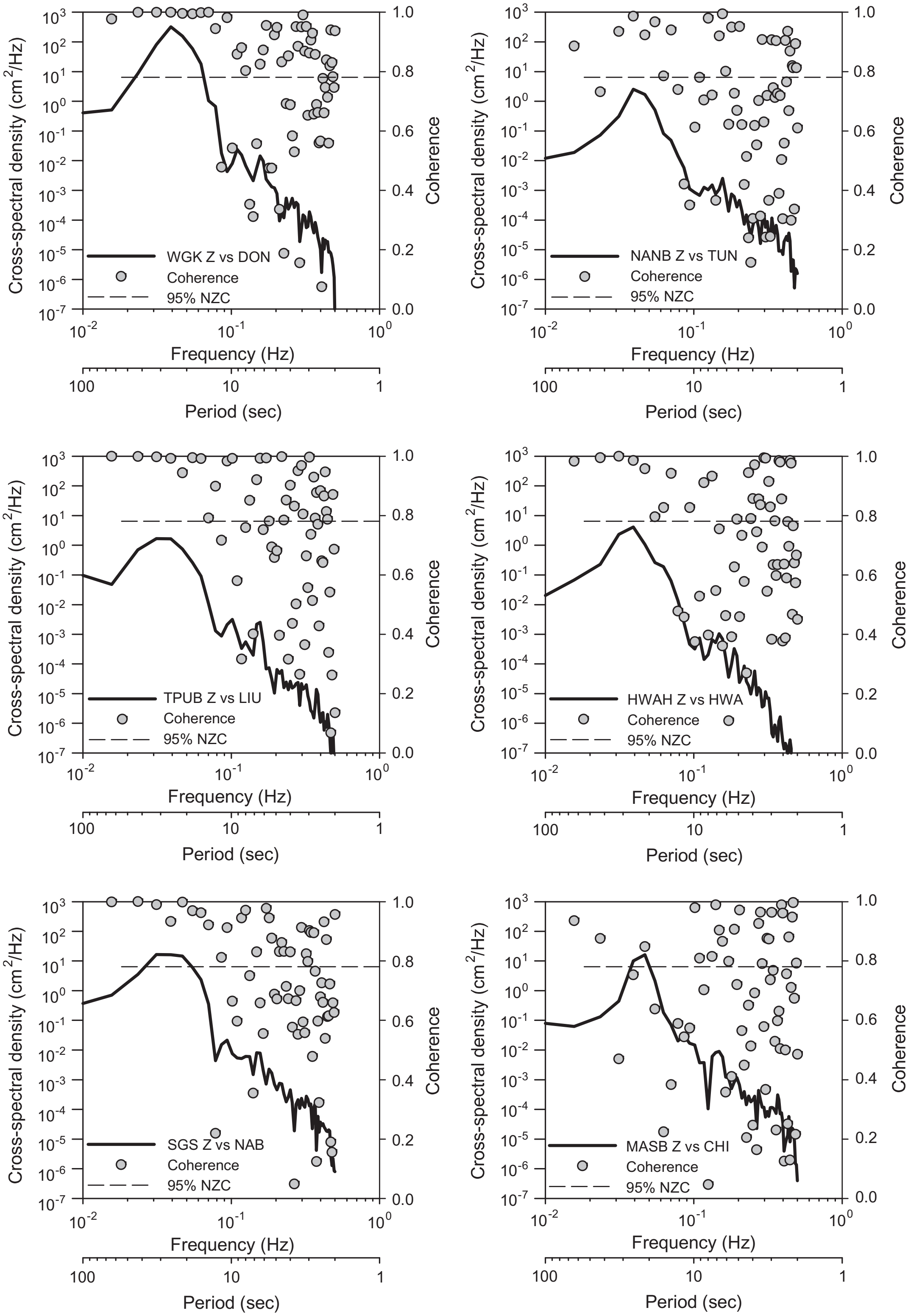

Fig. 8. Cross-spectral density in the frequency domain for groundwater level versus *Z* components of seismograms. The short dash lines indicate the 95% non-zero coherence level (NZC).

non-zero coherence level instead of the confidence interval (Shih et al., 1999).

Fig. 6 shows the autospectral density for groundwater and *x*–*Z* component in seismogram. Drastically, significant peaks for all groundwater with displacement observed in their control seismogram can be demonstrated. It implies that the periodic fluctuation of groundwater can be also observed in the component *x* and *Z* of seismogram. There are three dominant periods, i.e. 21.33, 25.6, and 32 s, were shown for station pair, respectively (Table 3). The cross-spectral density also represents very high coherence for *x*–*Z* components for those frequencies in seismogram (Fig. 7). For groundwater level and *Z* component of seismogram, it demonstrated distinctive high coherence in relevant frequency band (Fig. 8; Table 3). Coherence for MASB and CHI represent certain degree of lower coherence

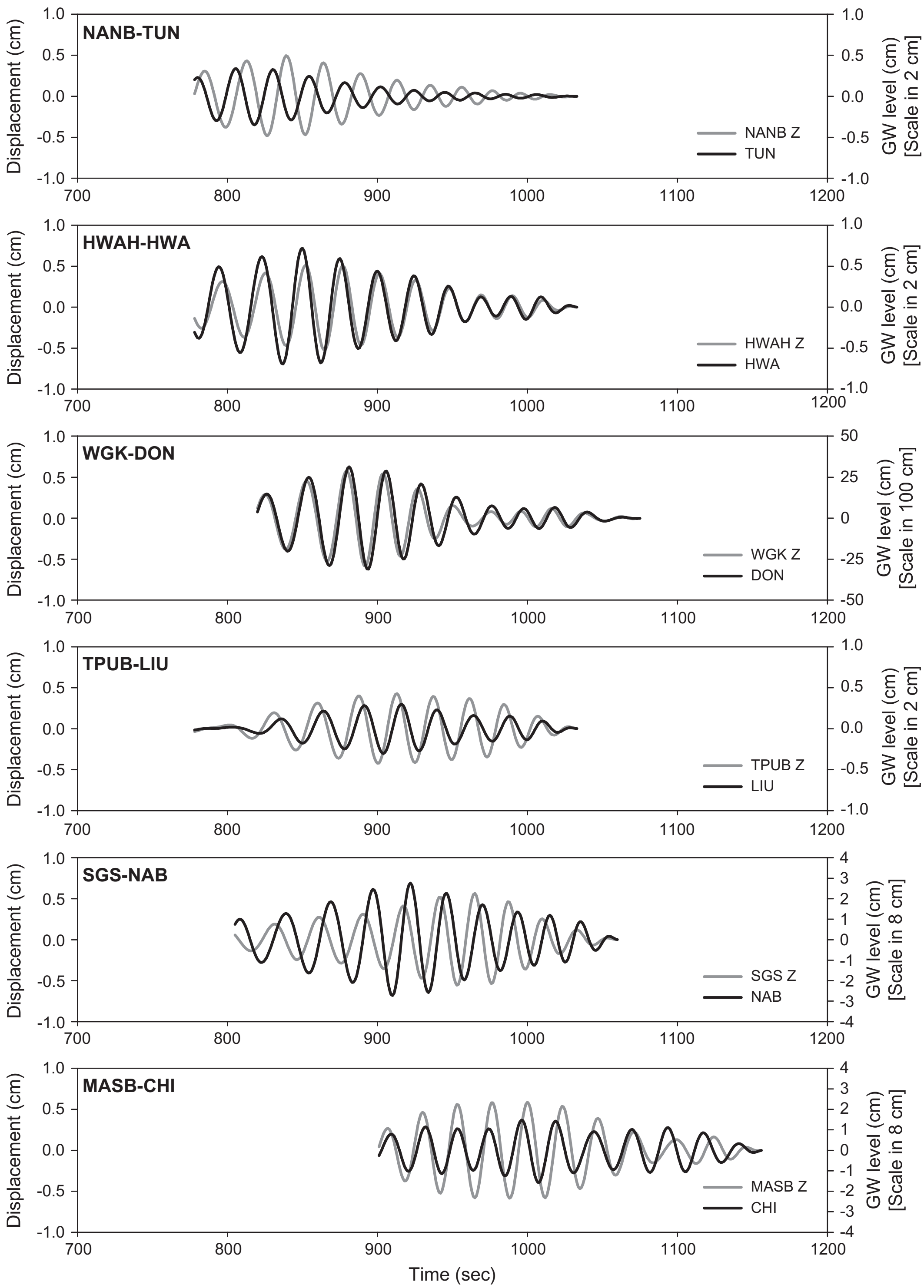

Fig. 9. Bandpass filter passing for 0.03–0.05 Hz (period 20–33 s) for groundwater and vertical component of seismogram.

than the other station pair. However, it is still significant as compared to non-zero significant coherence (NZC). Phase lag between groundwater and Z component can be estimated from cross-spectral density (Table 3). Owing to small departure between groundwater and seismic station, pair of MASB–CHI, WGK–DON and HWAH–HWA present small phase lag (Table 3; Fig. 1).

Note that groundwater level is highly coherent to the radial (x) and vertical (Z) components at period shown in Table 3. A bandpass filter of infinite impulse response (IIR) with zero phase at a frequency band 0.03–0.05 Hz (period 20–33 s) is applied to the groundwater time series and the seismograms (Fig. 9). The filtered time series of the groundwater level and vertical component of seismogram demonstrate a similar decay pattern. We suggest that groundwater fluctuations are sensitive and responsive to the vertical component of Rayleigh waves to momentous extent.

The harmonic wave components in a seismogram can be characterized by its amplitude A and two parameters, ω and k, that are angular frequency and wave number, respectively. Likewise, displacement is periodic in space over a distance equal to the wavelength $\lambda = 2\pi/k$. Frequency $f = 1/T = \omega/(2\pi)$ or by the angular

Table 4
Parameter of Rayleigh waves.

Station	Time to station for Rayleigh wave induced by Honshu event (s)	Distance to epicenter (km)	Velocity (km/s)	Period (s)	Frequency × 10^{-2} (s^{-1})	Wave length (km)
Groundwater						
TUN	778	2467.0874	3.1711	25.60	3.9063	81.1792
HWA	778	2539.1724	3.2637	25.60	3.9063	83.5512
DON	820	2639.6363	3.2191	25.60	3.9063	82.4082
LIU	778	2691.5048	3.4595	32.00	3.1250	110.7046
NAB	805	2703.7701	3.3587	32.00	3.1250	107.4791
CHI	901	2721.4318	3.0205	21.33	4.6875	64.4363
Seismogram						
NANB	778	2494.1718	3.2059	25.60	3.9063	82.0704
HWAH	778	2539.6216	3.2643	25.60	3.9063	83.5660
WGK	820	2639.6459	3.2191	25.60	3.9063	82.4085
TPUB	778	2664.8074	3.4252	32.00	3.1250	109.6065
SGS	805	2684.8307	3.3352	32.00	3.1250	106.7262
MASB	901	2718.5346	3.0172	21.33	4.6875	64.3677

frequency, $\omega = 2\pi f$, also can be estimated. Table 4 summarizes the wave parameters as concerned. Period and frequency is evaluated from the significant component in spectral density and resultant angular frequency, wave number and wave length can be obtained. The seismic signals and groundwater level at period of 21–32 s were significantly dominated by propagating Rayleigh waves. It shows the time from event to groundwater and seismic station for Rayleigh waves were ranged from 780 to 900 s while 3.0–3.5 km/s for wave velocity, 64–110 km for wave length. We group the station pair as four sets: (I) TUN/NANB and HWA/HWAH, eastern and northern region, station TUN located at ILan Plain, NANB located at rock basement, and HWA/HWAH located at Coastal Range (II) DON/WGK, western and central region, located at Coastal Plain (III) LIU/TPUB and NAB/SGS, western and southern region, located at Coastal Plain (IV) CHI/MASB, the most southern, extended region of Central Range (Fig. 1). For the most southern region for group (IV) wave travels more time from event to observation stations (Fig. 10a). It is clear that period, frequency and wave length for groups (I) and (II) sensed about same level without regarding distance to event (Fig. 10b and c). Groups (III) and (IV) demonstrate high and low period regarding the same distance to epicenter, respectively (Fig. 10b); this also can be found for wave length (Fig. 10c). Wave velocity for groups (I) and (II) demonstrate the same level (Fig. 10c); groups (III) and (IV) contrarily present high and low value, respectively. For the wave property observed in groundwater and seismograms (Fig. 10), groups (I) and (II) represent almost the same manner, even the Central Ridge divided them in eastern and western. However, groups (III) and (IV) drastically demonstrate different sense from groups (I) and (II) to high or low extreme.

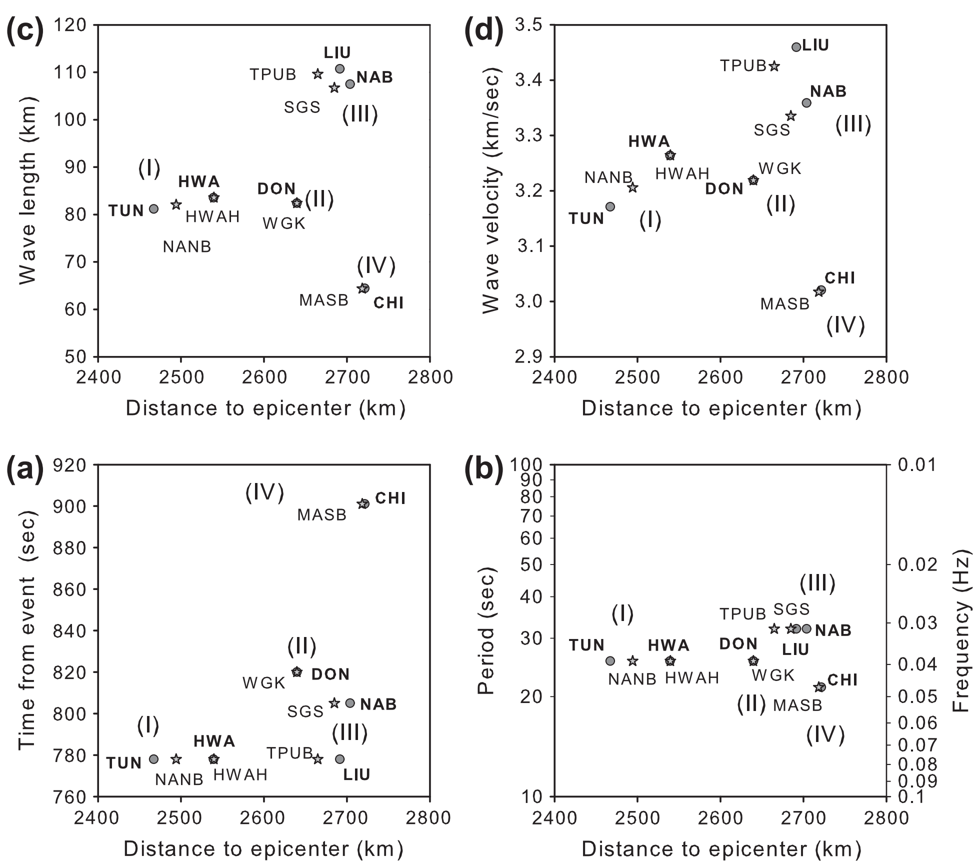

Fig. 10. Wave parameters versus distance to epicenter for groundwater and seismic stations.

However, our results show that the phenomenon of seismic wave-induced groundwater fluctuations can be well indentified using spectral analysis. Also, it accurately estimate the significant and coherent components between groundwater head and Rayleigh waves suggesting that fluctuations of groundwater are highly coherent with the radial and vertical components of Rayleigh wave motions. It appears that groundwater fluctuation is capable of responding to Rayleigh wave from a distant earthquake across over the intercontinental regions. Our identifications provide the valuable wave property for induced groundwater fluctuations from seismic surface wave.

5. Conclusion

This study demonstrates a field evidence of high coherence between groundwater fluctuations and seismic Rayleigh waves in the confined aquifer. It collected six sets of the groundwater fluctuations and seismic ground motions in Taiwan induced by the 2011 Tohoku earthquake in northern Honshu, Japan with magnitude of 9. Coherence of groundwater head to seismograms in both the time and frequency domains is further quantitatively evaluated using spectral analysis. The seismic signals and groundwater level at period of 21–32 s were significantly dominated by propagating Rayleigh waves. The analysis shows time from event to station for Rayleigh waves ranged from 780 to 900 s while 3.0–3.5 km/s for wave velocity, 64–110 km for wave length. Fluctuations of groundwater head are highly coherent with the vertical and radial components of Rayleigh wave motions. In no doubt, the relationship of groundwater fluctuations and ground motions induced by seismic activity become feasible to assess using spectral analysis. The resultant achievement can be performed to investigate aquifer characteristics in advances.

Acknowledgments

To complete this research, the authors thank Central Weather Bureau of Taiwan, Taiwan Earthquake Research Center, Institute of Earth Sciences/Academia Sinica and Water Resources Agency, MOEA, Taiwan for providing useful data; the support from Institute of Nuclear Energy Research (AEC) of Taiwan is also appreciated.

References

Barberopoulou, A., Qamar, A., Pratt, T.L., Steele, W.P., 2006. Long-period effects of the Denali earthquake on water bodies in the Puget Lowland: observations and modeling. Bull. Seismol. Soc. Am. 96 (2), 519–535.

Bendat, J.S., Piersol, A.G., 2000. Random Data, Analysis and Measurement Procedures. John Wiley, New York.

Bloomfield, P., 1976. Fourier Analysis of Time Series: An Introduction. John Wiley, pp. 80–87.

Chadha, R.K., Singh, Chandrani, Shekar, M., 2008. Short note: transient changes in well-water level in bore wells in Western India due to the 2004 M_w 9.3 Sumatra earthquake. Bull. Seismol. Soc. Am. 98 (5), 2553–2558.

Cooper, H.H., Bredehoeft, J.D., Papadopoulos, I.S., Bennett, R.R., 1965. The response of well-aquifer system to seismic waves. J. Geophys. Res. 70 (16), 3915–3926.

Google Earth, 2013. Google Earth Pro. Version: 5.2.1.1588 (Available on Febuary, 2013).

Ho, C.S., 1982. Tectonic Evolution of Taiwan. The Ministry of Economic Affairs, Republic of China, Taipei, Taiwan.

Lee, M., Liu, T.K., Ma, K.F., Chang, Y.M., 2002. Coseismic hydrological changes associated with dislocation of the September 21, 1999 Chichi earthquake, Taiwan. Geophys. Res. Lett. 29 (17), 1–5.

Lopes, R.H.C., Reid, I., Hobson, P.R., 2007. The two-dimensional Kolmogorov–Smirnov test. In: XI International Workshop on Advanced Computing and Analysis Techniques in Physics Research, Amsterdam, The Netherlands, April 23–27, 2007.

Peacock, J.A., 1983. Two-dimensional goodness-of-fit testing in astronomy. Mon. Not. R. Astron. Soc. 202, 615–627.

Robinson, E.S., Bell, R.T., 1971. Tides in confined well-aquifer system. J. Geophys. Res. 76 (8), 1857–1869.

Rotzoll, K., El-Kadi, A.I., Gingerich, S.B., 2008. Analysis of an unconfined aquifer subject to asynchronous dual-tide propagation. Ground Water 46 (2), 239–250.

Shapiro, S.S., Wilk, M.B., 1965. An analysis of variance test for normality (complete samples). Biometrika 52 (3–4), 591–611.

Shih, D.C.-F., 1999. Determination of hydraulic diffusivity of aquifers by spectral analysis. Stoch. Env. Res. Risk Assess. 13 (1–2), 85–99.

Shih, D.C.-F., 2009. Storage in a confined aquifer: spectral analysis of groundwater responses to seismic Rayleigh waves. J. Hydrol. 374, 83–91.

Shih, D.C.-F., Lin, G.-F., 2004. Application of spectral analysis to determine hydraulic diffusivity of a sandy aquifer (Pingtung County, Taiwan). Hydrol. Process. 18, 1655–1669.

Shih, D.C.-F., Chiou, K.-F., Lee, C.-D., Wang, I.-S., 1999. Spectral responses of water level in tidal river and groundwater. Hydrol. Process. 13, 889–911.

Shih, D.C.-F., Lin, G.-F., Jia, Y.-P., Chen, Y.-G., Wu, Y.-M., 2008a. Spectral decomposition of periodic groundwater fluctuation in a coastal aquifer. Hydrol. Process. 22, 1755–1765.

Shih, D.C.-F., Wu, Y.-M., Lin, G.-F., Chang, C.-H., Hu, J.-C., Chen, Y.-G., 2008b. Assessment of long-term variation in displacement for a GPS site adjacent to a transition zone between collision and subduction. Stoch. Env. Res. Risk Assess. 22 (3), 401–410.

Stein, S., Wysession, M., 2003. An Introduction to Seismology, Earthquakes, and Earth Structure. Blackwell Publishing.